Thesis Title: Fluorescence Sensing and Gas Sorption Properties of Water-Stable, Functionalized Metal-Organic Frameworks with Tetravalent Metal Ions and Carboxylate-Based Ligands

Name of the Candidate: Mr. Mostakim SK

Registration Number: 146122017

Thesis Supervisor: Dr. Shyam Prosad Biswas

Department: Chemistry

Institute: Indian Institute of Technology Guwahati, Guwahati, Assam, 781039, India.

Thesis Overview:

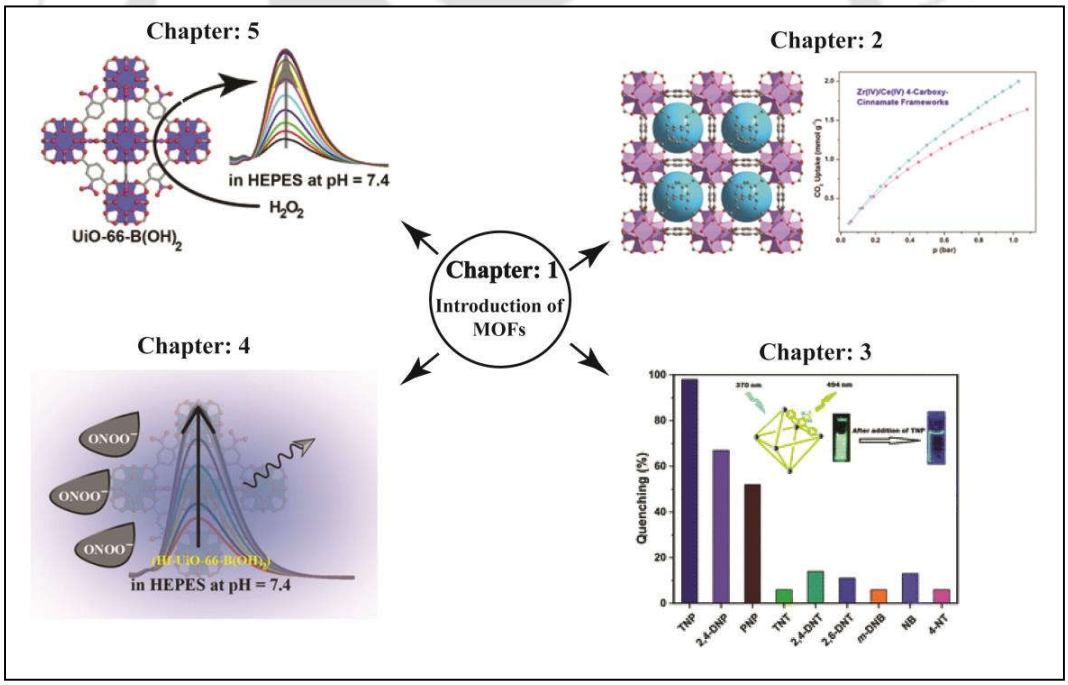

Chapter 1: Metal-organic frameworks (MOFs) are a new class of highly porous coordination polymers. They are interconnected by the inorganic building units and organic linkers in a 2D or 3D fashion. MOFs have emerged as a new class of highly crystalline materials over other traditional porous materials such as zeolites, silicas, activated carbons, etc. MOFs have large surface areas and permanent porosity. Extending

the length of organic linkers leads to increase in pore sizes for the resulting MOFs. Attaching hydrophobic functional groups with the organic linkers enhances hydrophobicity of the MOFs. The tuneable functionality and precise arrangement of the organic linkers make them potential candidates for selective gas adsorption, separation, chemical sensing, proton conductivity, electrical conductivity, heterogeneous catalysis, photo-catalysis, drug delivery, etc. The MOF-based fluorescence sensing results from the incorporation fluorescent linkers or incorporation of f-block metal ions. Post-synthetic modification of MOFs also enhances some additional properties in chemical sensing, drug delivery, gas sensing, chemical stability, etc. Due to the formation of strong bonds between metal ions (specially in high oxidation states) and carboxylate groups of organic linkers, the resulting MOF materials show high thermal and chemical stability, which are desirable for practical applications such as gas adsorption and chemical sensing. Inspired by the above-mentioned advantages, a broad variety of MOF materials have been investigated for gas storage as well sensing of a wide range of analytes including cations, anions, biomolecules, small molecules, volatile organic compounds and nitro explosive materials.

Chapter 2 presents two different types of Zr(IV) and Ce(IV)-based MOFs having the same crystal structure. The compounds were synthesized under solvothermal conditions by using 4-carboxycinnamic acid (H_2CCA). Zr-MOF (**1**) was synthesized from a mixtures of $ZrCl_4$, H_2CCA ligand and acetic acid with a molar ratio of 1:1:10 in DMF at 150 °C for 24 h. Ce-MOF (**2**) was synthesized by solvothermal reaction of a mixture of ammonium cerium(IV) nitrate and H_2CCA ligand in a DMF/H_2O mixture at 100 °C for 20 min. The as-synthesized and activated forms (**1′** and **2′**) of the compounds were characterized by XRPD (Figures 1 and 2), FT-IR, TG and elemental analysis. The TG analysis revealed that **1** and **2** show high thermally stable up to 390 and 300 °C in air atmosphere, respectively. The chemical stability of both compounds were characterized by XRPD measurements. Both compounds showed moderate stability in water, but they lost their crystallinity in 1 M HCl. N_2 sorption experiments revealed that **1′** and **2′** possess BET surface areas of 870 and 1210 $m^2\ g^{-1}$, respectively (Figure 3). The CO_2 uptake values of **1′** and **2′** at 0 °C and 1 bar were 2.0 and 1.6 mmol g^{-1}, respectively.

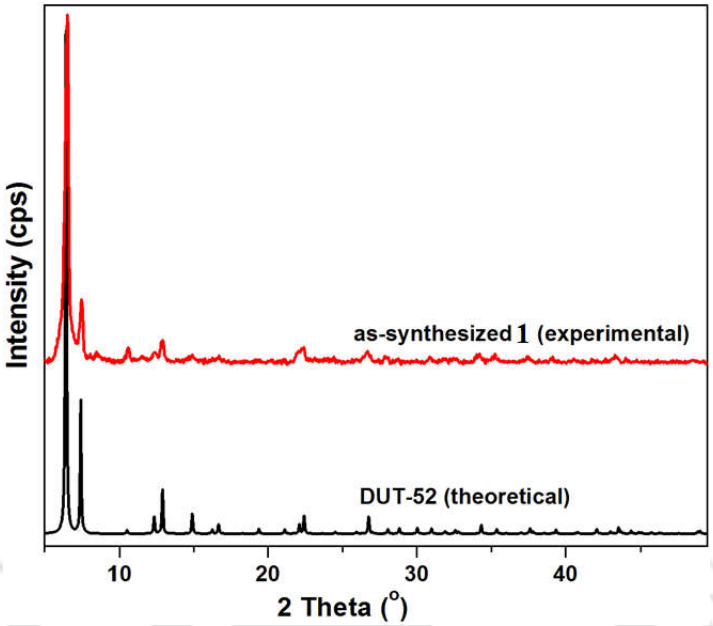

Figure 1. Theoretical (black) XRPD pattern of DUT-52 and experimental (red) XRPD pattern of as-synthesized compound **1**. (*Microporous Mesoporous Mater.*, 2017, **237**, 275-281)

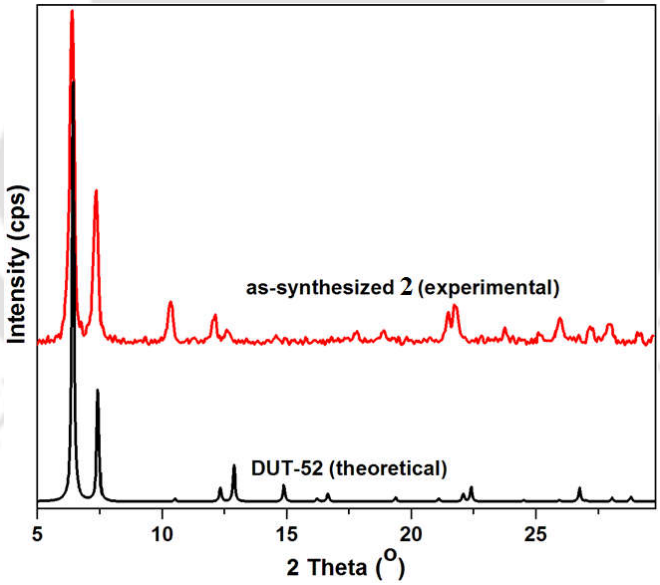

Figure 2. Theoretical (black) XRPD pattern of DUT-52 and experimental (red) XRPD pattern of as-synthesized compound **2**. (*Microporous Mesoporous Mater.*, 2017, **237**, 275-281)

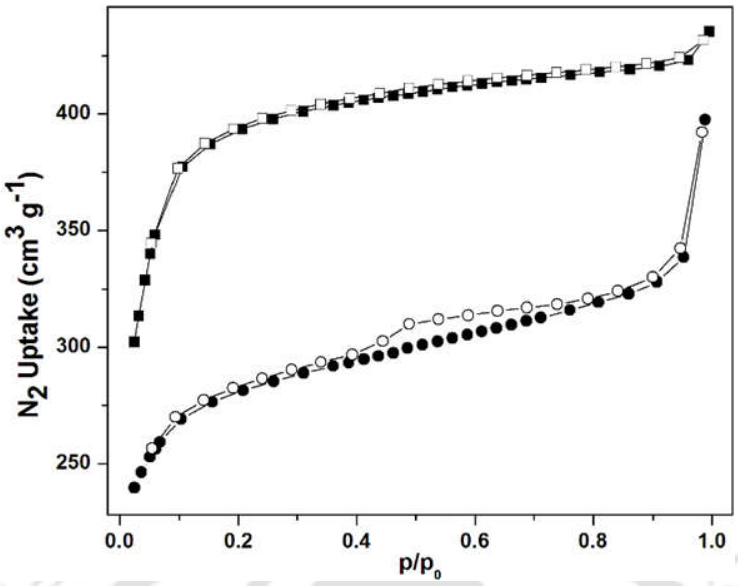

Figure 3. N_2 adsorption (filled symbols) and desorption (empty symbols) isotherms of **1′** (circles) and **2′** (squares) measured at –196 °C. (*Microporous Mesoporous Mater.*, 2017, **237**, 275-281)

Chapter 3 presents a new fluorescent MOF called Zr-BTDB which was synthesized by using H_2BTDB {H_2BTDB = 4,4′-(benzo[*c*][1,2,5]thiadiazole-4,7-diyl)dibenzoic acid} ligand. Zr-BTDB was prepared under solvothermal conditions from a mixture of $ZrCl_4$, H_2BTDB and trifluoroacetic acid (used as a modulator) in DMF at 150 °C for 24 h. The as-synthesized material (**3**) was characterized by XRPD analysis, FT-IR spectroscopy and elemental analysis. The thermal stability of **3** was envisaged by using TG analysis which revealed that **3** is stable up to 400 °C. The activated form (called **3′**) of **3** was obtained by solvent exchange with methanol, followed by heating under high vacuum. XRPD experiments verified that the activated **3′** retained its crystallinity when exposed to water, acetic acid and 1 M HCl solutions. From the steady-state fluorescence titration experiments of the activated compound **3′**, showed a selective sensing behavior towards 2,4,6-trinitrophenol (TNP, commonly known as picric acid) (Figure 4), even in the presence of other potentially competing explosive nitroaromatic compounds (Figure 5). The detection limit of **3′** was 1.63×10^{-6} M. The fluorescence quenching ability of TNP can be ascribed to both energy and electron transfer processes as well as electrostatic interactions between the hydroxyl group of TNP and the Lewis basic N-donor sites of the BTDB ligand in the structural framework.

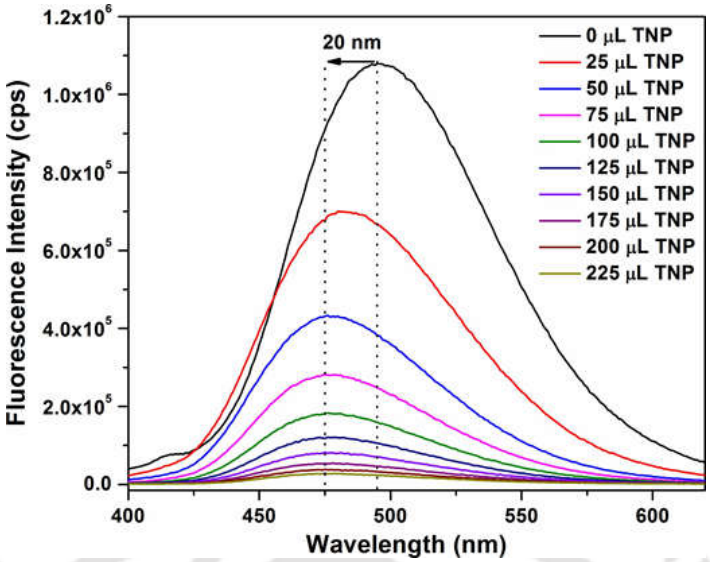

Figure 4. Quenching of the fluorescence intensity of **3′** by gradual addition of 3 mM TNP solution to a 3 mL well-dispersed methanol suspension of **3′** (λ_{ex} = 370 nm and λ_{max} = 494 nm). (*CrystEngComm*, 2016, **18**, 3104-3113)

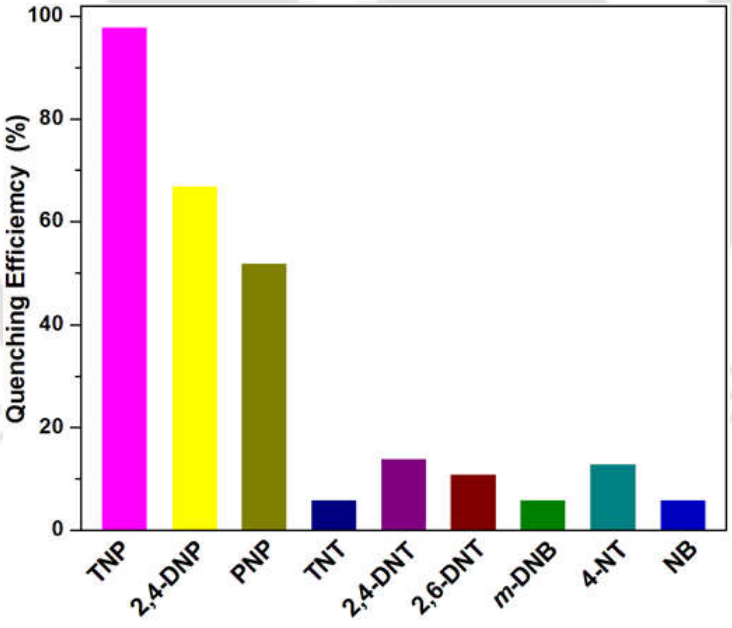

Figure 5. Fluorescence quenching efficiencies of various nitroaromatic explosives towards **3′** at 3 mM concentration (λ_{ex} = 370 nm and λ_{max} = 494 nm). (*CrystEngComm*, 2016, **18**, 3104-3113)

Chapter 4 presents a boronic acid functionalized Hf-based MOF called UiO-66-B(OH)$_2$ which has capability of selectively sensing of $ONOO^-$ in live cells. Hf-UiO-66-B(OH)$_2$ MOF was synthesized from a mixture of $HfCl_4$ and 2-borono-1,4-benzenedicarboxylic

acid [$H_2BDC–B(OH)_2$] ligand in DMF in the presence of formic acid at 130 °C for 48 h. The phase purity of the as-synthesized material (**4**) was confirmed by comparison of XRPD pattern of **4** with the XRPD pattern of Hf-based UiO-66 framework (Figure 6). The as-synthesized material (**4**) was activated by exchange with methanol, followed by heating under high vacuum. The activated material (**4′**) was utilized as a fluorescent turn-on probe for the rapid sensing of extracellular peroxynitrite ($ONOO^-$) under conditions mimicking those of biological medium (10 mM HEPES buffer, pH 7.4) (Figure 7). Selective sensing of $ONOO^-$ over other ROS/RNS was also achieved by **4′** (Figure 8). The selective turn-on sensing behavior towards $ONOO^-$ can be ascribed to the oxidative cleavage of attached boronic acid groups forming corresponding hydroxy-functionalized ligands. The probe showed extraordinary sensitivity (detection limit = 9.0 nM) toward $ONOO^-$ in 10 mM HEPES buffer at pH 7.4. The probe-loaded cells did not affect the cellular cytotoxicity and morphological deformities. It is remarkable that the probe inside the cells responded toward the $ONOO^-$ solution to give an intense blue fluorescent signal. The fluorescence microscopy study with J774A.1 macrophage cells unambiguously demonstrated that probe **4′** is suitable to image peroxynitrite in living cells (Figure 9).

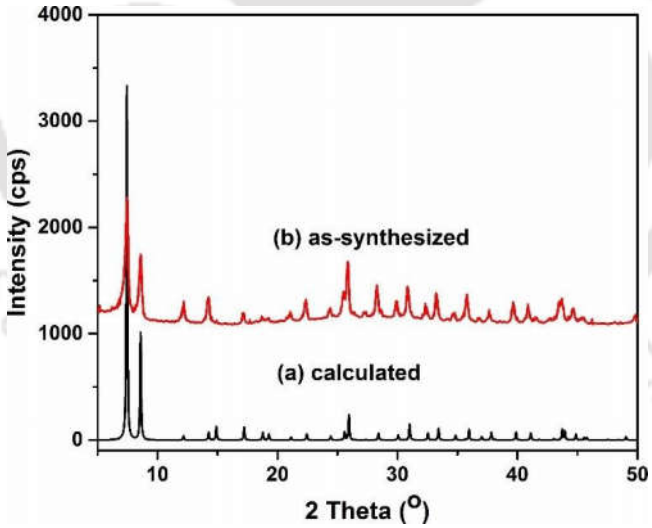

Figure 6. Comparison between (a) calculated XRPD pattern of Hf-UiO-66 and (b) experimental XRPD pattern of as-synthesized **4.** (*Inorg. Chem.*, 2018, **57**, 10128-10136)

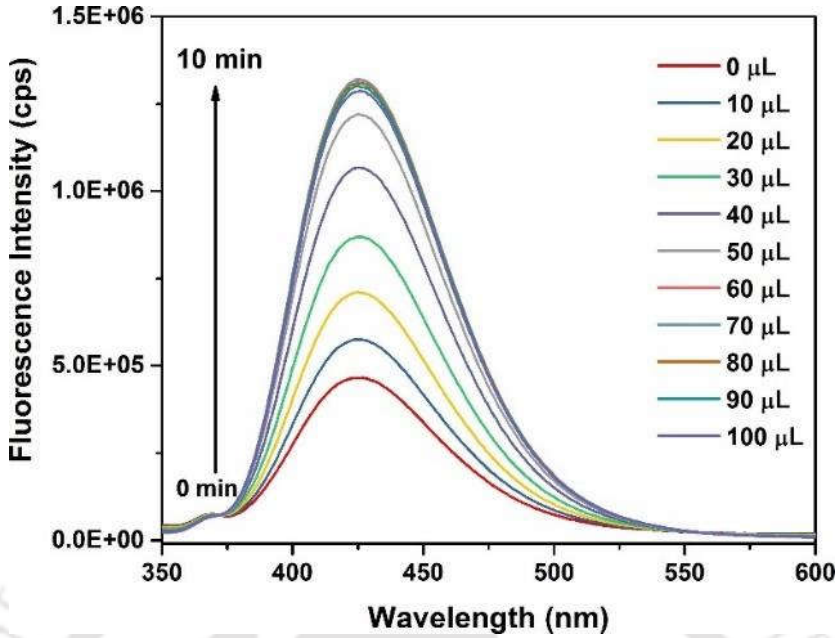

Figure 7. Selective turn-on response of **4′** (in 10 mM HEPES buffer at pH = 7.4) upon incremental addition of 0.5 mM $ONOO^-$ solution. (*Inorg. Chem.*, 2018, **57**, 10128-10136)

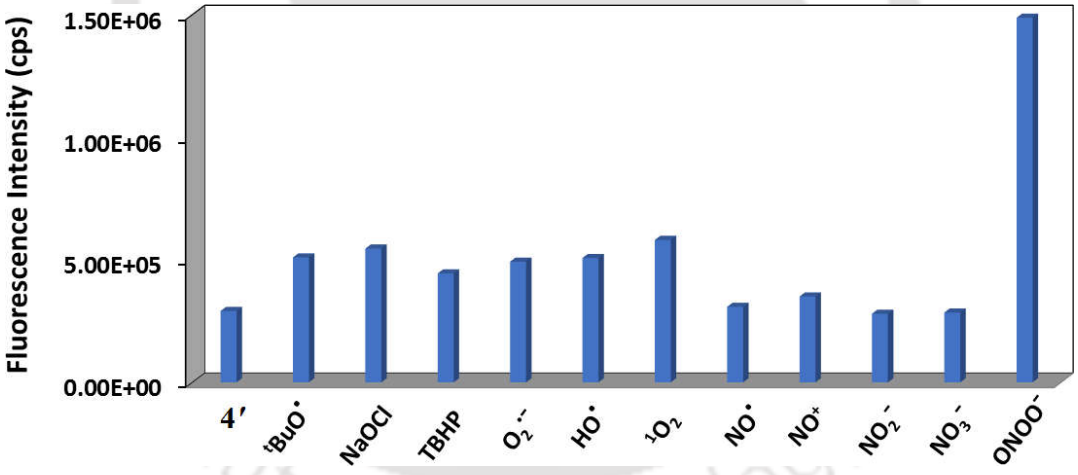

Figure 8. Comparative fluorescence enhancement behavior of **4′** in HEPES buffer (10 mM, pH = 7.4) towards different ROS/RNS (**4′**, 0.5 mM of $^tBuO^•$, NaOCl, TBHP, $O_2^{•-}$, $HO^•$, $^1O_2$, $NO^•$, NO^+, NO_2^-, NO_3^- and $ONOO^-$) (λ_{ex} = 330 nm and λ_{em} = 426 nm). (*Inorg. Chem.*, 2018, **57**, 10128-10136)

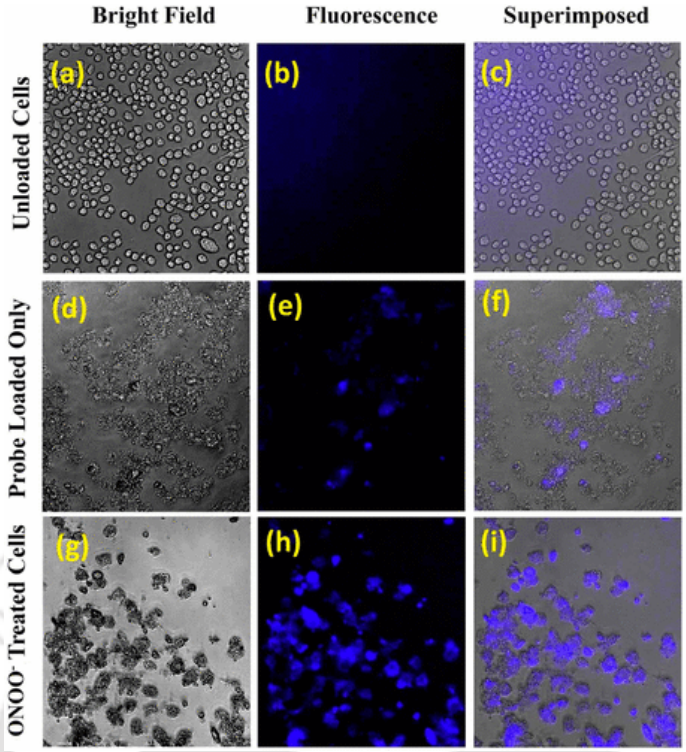

Figure 9. Sensing of $ONOO^-$ in J774A.1 macrophage cells using **4′**. Bright-field (a, d, g) and fluorescence channel (b, e, h) images as well as their superposition (c, f, i) are shown for the unloaded cells, probe-loaded cells, and probe-loaded cells after treatment with $ONOO^-$. Remarkably, the cells loaded with probe **4′** (5 μM) showed bright blue fluorescence after treatment with $ONOO^-$ (50 μM) solution (h, i). (*Inorg. Chem.*, 2018, **57**, 10128-10136)

Chapter 5 demonstrates a new boronic acid ($H_2BDC\text{-}B(OH)_2$) functionalized Zr(IV) metal-organic framework (Zr-UiO-66-$B(OH)_2$) having the capability of sensing H_2O_2 in live cells. XRPD analysis revealed that the structure of as-synthesized material (**5**) was similar as the UiO-66 framework (Figure 10). The activated material was denoted as **5′**. Compound **5′** was highly selective for fluorogenic detection of H_2O_2 in 10 mM HEPES buffer at pH = 7.4 (Figure 11), even in the presence of interfering ROS (ROS = reactive oxygen species) and other biologically relevant analytes (Figure 12). The fluorescent probe was found to display extraordinary sensitivity for H_2O_2 (detection limit = 0.015 μM) in HEPES buffer, which represents lower value than the MOF probes documented so far for sensing H_2O_2 using other analytical methods. For high selectivity and sensitivity of H_2O_2 in HEPES buffer, the probe was employed for the imaging of intracellular H_2O_2. Imaging studies with MDAMB-231 cells revealed the emergence of bright blue fluorescence after loading with probe **5′** and subsequent treatment with H_2O_2 solution (Figure 13).

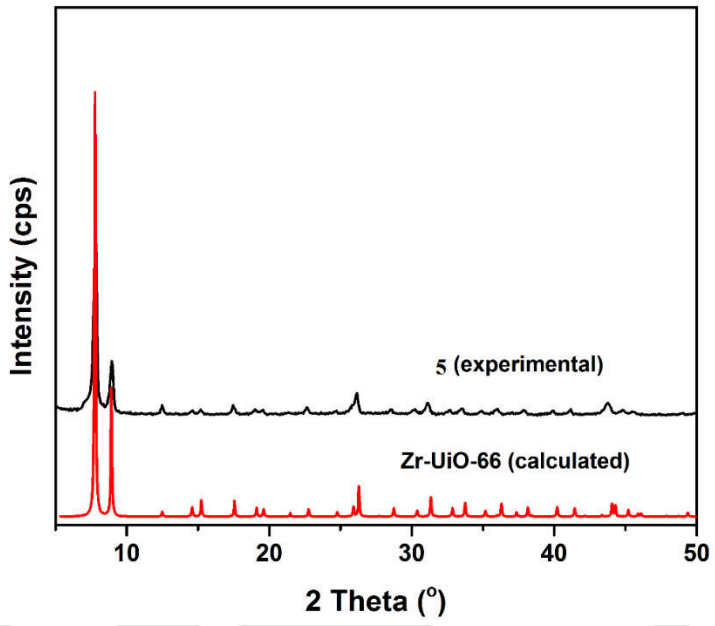

Figure 10. Comparison between the experimental XRPD pattern of **5** and calculated XRPD pattern of Zr-UiO-66. (*Inorg. Chem.*, 2018, **57**, 14574–14581)

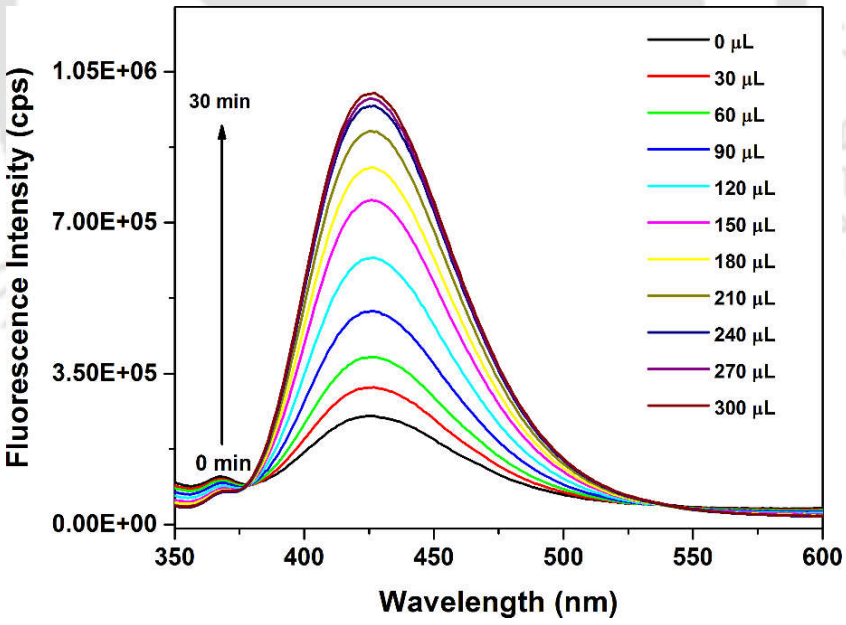

Figure 11. Fluorescence turn-on response of **5′** (suspended in 10 mM HEPES buffer, pH = 7.4) upon the stepwise addition of 10 mM H_2O_2 solution at room temperature. The spectra were collected after 3 min of each addition. (*Inorg. Chem.*, 2018, **57**, 14574–14581)

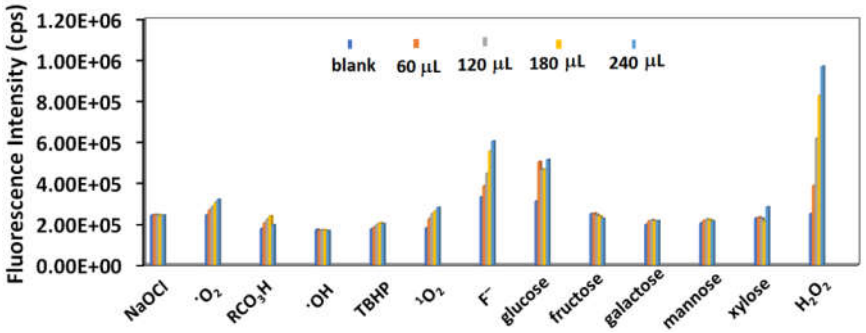

Figure 12. Fluorescence responses of **5′** (suspended in 10 mM HEPES buffer, pH = 7.4) upon the addition of solutions of various ROS (10 mM of ClO^-, $O_2^{\bullet-}$, $^tBuO^\bullet$, $HO^\bullet$, TBHP, $^1O_2$ and H_2O_2) and other biologically relevant species (10 mM of F^-, glucose, fructose, galactose, xylose and mannose) at room temperature. The bars denote fluorescence intensity after the addition of blank, 60, 120, 180 and 240 µL of each ROS. The spectra were collected after 6 min of each addition. (*Inorg. Chem.*, 2018, **57**, 14574–14581)

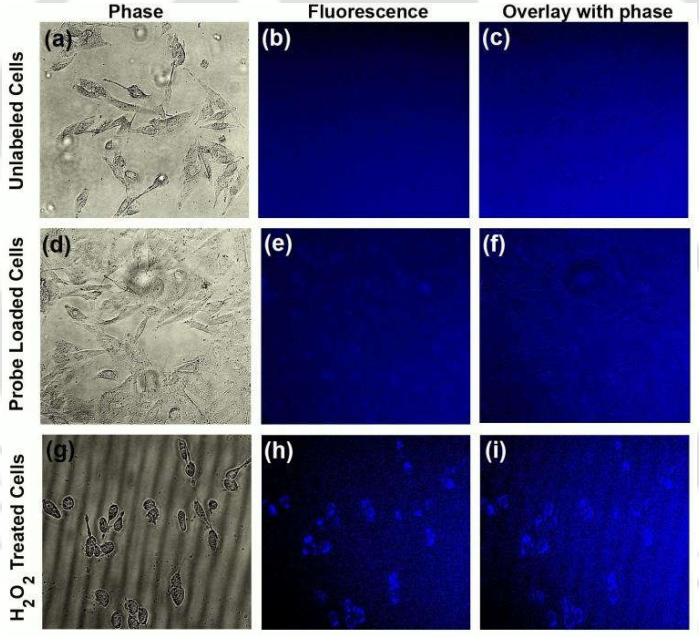

Figure 13. Detection of H_2O_2 inside the MDAMB-231 cells loaded with probe **5′**. The panel (a-c) is the unlabeled cells, (d-f) denotes probe-loaded cells and (g-i) represents probe-loaded cells treated with H_2O_2. The cells either remained unloaded (a-c) or probe (5 µM) loaded cells either remained untreated (d-f) or treated (g-i) with H_2O_2 (1 µM) for 5 min at 37 °C. The H_2O_2-treated cells showed bright blue fluorescence as compared to the probe-loaded cells. An overlay of bright field and fluorescence images indicates that the fluorescence is arising from the cell. (*Inorg. Chem.*, 2018, **57**, 14574–14581)